Asian Journal of Chemistry; Vol. 38, No. 7 (2026), 1921-1929
ASIAN JOURNAL OF CHEMISTRY
https://doi.org/10.14233/ajchem.2026.35811

Synthesis, Physico-chemical Characterisation and Biomedical Applications of Diols and Citric Acid based Indole-3-Acetic Acid Polyester Hydrogels

G. CHITRA[1,*], S. GUHANATHAN[2], K. SUBASHINI[3] and P. RAMKUMAR[4]

[1]Department of Chemistry, Government Polytechnic College, Kelamangalam, Krishnagiri-635113, India
[2]Department of Chemistry, Muthurangam Government Arts College (Affiliated to Thiruvalluvar University, Serkadu), Vellore-632002, India
[3]Department of Chemistry, Applied Sciences, New Horizon College of Engineering, Bangalore-560103, India
[4]Department of Computer Science and Engineering, Sri Sairam College of Engineering, Bangalore-562106, India

*Corresponding author: E-mail: chitramuralikrishnan@gmail.com

Received: 23 February 2026 *Accepted*: 20 June 2026 *Published online*: 3 July 2026 AJC-22417

In this work, indole-3-acetic acid (IAA)-based polyester hydrogels were synthesized using citric acid and three different diols, namely ethylene glycol, diethylene glycol and triethylene glycol, to obtain ICAE, ICAD and ICAT hydrogels. The synthesized hydrogels were characterized by FT-IR, ^{1}H NMR, SEM, TGA and swelling studies, confirming successful hydrogel formation and structural integrity. All hydrogels exhibited pH-dependent swelling behaviour, with ICAE showing the highest swelling equilibrium (1600% at pH 3). Biological evaluation revealed concentration-dependent antifungal activity, excellent biocompatibility with cell viability above 80% and significant wound-healing potential. Among the formulations, ICAE demonstrated superior antifungal efficacy, 75% wound closure after 72 h and the strongest anticancer activity against A549 cells with an IC_{50} value of 138 µg/mL. The enhanced performance of ICAE was attributed to its higher swelling capacity and favourable biological properties. These results suggest that ICAE is a promising multi-functional hydrogel for wound management and anticancer biomedical applications.

Keywords: Heterocyclic hydrogel, Diols, Wound healing, FT-IR, Anticancer activities.

INTRODUCTION

Hydrogels are the three-dimensional networks of cross-linked hydrophilic polymers capable of absorbing large quantity of water while maintaining their structural integrity [1]. Depending on the nature of the crosslinks, hydrogels may be chemically or physically crosslinked through covalent, ionic, hydrogen bonding or entanglement interactions [2]. Due to their unique ability to respond to external stimuli such as pH, temperature, light, magnetic fields and ionic strength, smart hydrogels have attracted considerable attention in pharmaceutical and biomedical applications [3]. Natural biopolymers are increasingly employed for the fabrication of intelligent hydrogels because of their biocompatibility, biodegradability, non-toxicity, renewability and ease of chemical modification [4]. Significant efforts have been directed toward developing renewable resource-based hydrogels with pH-responsive and antimicrobial properties using environmentally benign monomers [5,6].

Indole-3-acetic acid (IAA) is a biologically important indole derivative involved in plant growth regulation and cellular differentiation processes [7-9]. It is also a major tryptophan metabolite produced by intestinal microorganisms in animals [10,11]. Citric acid, an inexpensive and multi-functional renewable monomer, has been widely investigated due to its excellent reactivity and ability to participate in hydrogen-bonding interactions within polyester networks [12-14]. Diethylene glycol, a bifunctional linear diol, contributes flexibility, biocompatibility and improved hydrogel performance, while indole derivatives are known for their antioxidant, antimicrobial and low-toxicity characteristics [15]. Several researchers has previously reported pH-sensitive biopolymeric hydrogels containing aliphatic segments [16-18]. The physical properties, swelling behaviour and hydrophilic-hydrophobic balance of hydrogels can be effectively tuned through the selection of suitable diols and acids [19].

Oxidative stress caused by excessive free radical production is associated with numerous degenerative disorders when endogenous antioxidant defenses become insufficient [20]. Polycondensation of diols with multifunctional renewable monomers offers several advantages, including simple synth-

esis, catalyst-free processing, elimination of toxic crosslinkers and improved control over material performance [21,22]. Furthermore, incorporation of unsaturated monomers enables additional crosslinking through free-radical reactions [23]. In wound management, bacterial infections frequently delay healing and may lead to chronic complications [24,25]. Although antibiotics have significantly reduced infection-related mortality since the discovery of penicillin [26], the emergence of antimicrobial resistance has created an urgent need for alternative therapeutic materials. Hydrogels are attractive wound dressings since they are biocompatible, biodegradable, moisture-retentive and capable of delivering bioactive agents directly to the wound site [27,28]. Incorporation of antioxidant and antibacterial components including metal nano-oxides and cationic compounds, can further promote tissue regeneration and reduce bacterial colonization [29-33].

Diol-based hydrogels contain hydroxyl-functionalized building blocks that participate in network formation and can impart self-healing, injectability and stimulus-responsive behaviour. Their excellent biocompatibility and biodegradability make them particularly suitable for biomedical applications. Since chronic wounds remain a major healthcare challenge worldwide [31,34-37], the development of multifunctional hydrogel systems with enhanced healing properties is of considerable interest. Moreover, advanced biomaterials capable of supporting cancer therapy and improving patient outcomes are increasingly sought after [38].

The novelty of the present work lies in the comparative synthesis and systematic evaluation of heterocyclic hydrogels prepared using different diols to investigate the influence of diol chain length and molecular flexibility on hydrogel performance. Unlike previous studies focused on the single formulations, this work examines structure-property relationships in terms of swelling behaviour, porosity, biodegradability, mechanical characteristics and biomedical functionality. The incorporation of heterocyclic moieties and tunable diol segments provides enhanced control over network architecture, crosslinking density, stability and biocompatibility. Accordingly, indole-3-acetic acid-based hydrogels were synthesized through condensation polymerization and evaluated for their wound-healing and anticancer potential. Their pH-dependent swelling behaviour was investigated and the resulting hydrogels were characterized using Fourier transform infrared (FT-IR) spectroscopy and field emission scanning electron microscopy (FESEM).

EXPERIMENTAL

Anhydrous citric acid (CA) was obtained from S.D. Fine Chemicals, India. Ethanol, ethylene glycol, diethylene glycol and triethylene glycol were obtained from Merck Ltd., India. The monomer indole-3-acetic acid was sourced from Sigma-Aldrich Chemical Company, India. De-mineralised water was used for polymerization and for preparing buffer solutions.

Synthesis of biopolymeric hydrogels: The synthesis of biopolymeric hydrogels is accomplished through a two-step synthetic process involving successive chemical reactions.

Synthesis of pre-polymers: Citric acid was dissolved in ethanol in a round bottom flask, fitted with condenser tube on the mechanical stirrer and nitrogen inlet. Ethylene glycol/diethylene glycol/triethylene glycol was added in a dropwise in separate vessels. The content was stirred for 1 h at room temperature in round bottom flask kept in silica oil bath at 160 ºC under nitrogen atmosphere. The completion of the reaction was observed by the formation of white colour sticky gel like compound. The resultant compound was labelled as CAE or CAD or CAT.

Synthesis of biopolymeric hydrogels: The hydrogels were synthesised according to our reported method [5]. In brief, indole-3 acetic acid (IAA) was dissolved in ethanol and poured into pre-polyester (CAE) in a silica oil bath at 160 ºC for 3 h under N_2 atmosphere. The high viscous reddish-brown compound indicated the end of the reaction. The resultant compound cooled down at room temperature to form reddish brown glassy gel. The gel was submerged in distilled water for 24 h to remove the unreacted monomers. Then, the gel was placed in a warm oven for 24 h, to remove the moisture and this formed sticky gel (ICAE) with 85% yield. Using the same synthetic method, the other hydrogels were also prepared with different diols to obtain the corresponding ICAD and ICAT.

$$\text{Yield (\%)} = \frac{\text{Actual yield}}{\text{Theoretical yield}} \times 100$$

where actual yield = weight of dried hydrogel obtained experimentally, and theoretical yield = calculated maximum possible weight based on the starting materials.

Characterisation: FT-IR spectra of the hydrogels and nanocomposite hydrogels were recorded using KBr pellets on a Shimadzu FTIR-8400S spectrophotometer over the range of 4000-400 cm^{-1}. ^1H NMR and ^{13}C NMR spectra were obtained in DMSO-d_6 using a Bruker AVANCE III spectrometer operating at 250 MHz and 62.5 MHz, respectively, with tetramethylsilane (TMS) as the internal standard. Thermal properties were evaluated using a Q20 DSC and SDT Q600 thermal analyzer; thermogravimetric analysis (TGA) was performed from room temperature to 800 ºC at a heating rate of 10 ºC min^{-1} under a nitrogen atmosphere. The surface morphology of the samples was examined using a Hitachi SU6600 field emission scanning electron microscope (FESEM).

Swelling studies: The swelling behavior of the hydrogel was investigated in buffer solutions of varying pH (3.0-10.0) at room temperature. Pre-weighed dried hydrogel samples were immersed in the respective buffer solutions and the pH was verified using a pH meter (Systronics 3300, India). The swollen hydrogels were removed at regular intervals, initially every 30 min for up to 6 h, and subsequently monitored until equilibrium swelling was attained. To determine the equilibrium swelling capacity, the samples were allowed to remain immersed for 48 h. The degree of swelling and equilibrium swelling ratio were calculated using eqn. 1:

$$S_{eq}(\%) = \frac{W_{eq} - W_d}{W_d} \times 100 \quad (1)$$

where W_d and W_{eq} are the weights of the sample before and after swollen at equilibrium, respectively.

Biological activities

Antifungal assay: The antifungal activity of the synthesised hydrogels was evaluated against selected fungal strains, namely *Aspergillus fumigatus*, *Candida albicans* and *Rhizopus oryzae* using the agar well diffusion method. The hydrogels were tested at concentrations of 500, 1000, 1500 and 2000 μg mL^{-1}. Fungal cultures were grown on dextrose agar plates at 27 ºC for 72 h and the fungal inoculum was prepared by aseptically collecting spores/cells using a sterile brush. Subsequently, 100 μL of the fungal suspension was uniformly spread onto fresh dextrose agar plates. Wells were then developed in the agar medium, and the test samples at different concentrations were added using sterile pipettes. The plates were allowed to stand at room temperature for 2 h to facilitate diffusion of the samples into the agar and were subsequently incubated at 27 ºC for 48 h. Ketoconazole (10 μg) and DMSO served as the positive and negative controls, respectively. Antifungal activity was assessed by measuring the diameter of the inhibition zones around the wells.

Cytotoxicity assay: The cytotoxicity of the samples was evaluated using the MTT assay in 96-well plates. Cells were seeded and treated with the test samples in a final volume of 100 μL per well, followed by incubation for the desired exposure period. Subsequently, 10 μL of MTT solution was added to each well to achieve a final MTT concentration of 0.45 mg mL^{-1} and the plates were incubated at 37 ºC for 1-4 h. After the formation of formazan crystals, 100 μL of solubilisation solution was added to each well and mixed thoroughly to ensure complete dissolution. The absorbance was then measured at 570 nm using a microplate reader, and cell viability was calculated relative to the untreated control.

Scratch wound healing assay (*in vitro*): Cells were cultured in Dulbecco's Modified Eagle Medium (DMEM) supplemented with 10% fetal bovine serum (FBS) and seeded into 24-well tissue culture plates. After 24 h of incubation, when the cells reached approximately 70-80% confluence, a linear scratch was created across the center of each well using a sterile 1 mL pipette tip. Detached cells were removed by washing twice with phosphate-buffered saline (PBS) and fresh medium was added. The cells were then incubated for an additional 48 h to allow migration into the wound area. Following incubation, the cells were washed twice with PBS, fixed with 3.7% paraformaldehyde for 30 min and stained with 1% crystal violet prepared in 2% ethanol for 30 min. Images of the stained cell monolayers were subsequently captured using an optical microscope to evaluate cell migration and wound closure.

Anticancer activity: The *in vitro* anticancer activity of the synthesised biopolymer hydrogels was evaluated against human lung carcinoma (A549), breast adenocarcinoma (MDA-MB-231) and prostate carcinoma (PC3) cell lines using the MTT assay. Cells were seeded in 96-well plates and treated with varying concentrations of the test samples for 24 h in a final volume of 100 μL per well. Following treatment, 10 μL of MTT solution was added to each well to achieve a final concentration of 0.45 mg mL^{-1} and the plates were incubated at 37 ºC for 1-4 h. The resulting formazan crystals were dissolved by adding 100 μL of solubilization solution to each well. After complete dissolution, absorbance was recorded at 570 nm using a microplate reader. Cell viability was expressed as a percentage relative to untreated control cells and the IC_{50} values were determined from dose–response curves.

RESULTS AND DISCUSSION

FT-IR spectral studies: The FT-IR spectrum of ICAE (Fig. 1) exhibited a characteristic band at 1630 cm^{-1}, corresponding to the carboxyl (C=O) group of citric acid. The appearance of a strong absorption band at 1720 cm^{-1} confirmed the formation of ester linkages through C=O stretching vibrations [39]. The bands observed at 1095 and 1027 cm^{-1} were attributed to C–O–C stretching vibrations, while the peak at 1458 cm^{-1} corresponded to the stretching vibration of the COO^- group. Characteristic absorption bands associated with methylene (-CH_2-) groups of the constituent diacids and diols were also evident in the spectrum [40,41]. The successful incorporation of indole-3-acetic acid (IAA) into the ICAE hydrogel was confirmed by the band at 1648 cm^{-1}, assigned to aromatic C=C stretching of the indole ring, and the peak at 744 cm^{-1}, corresponding to out-of-plane C–H bending vibrations of the indole moiety. A broad absorption band centered around 3400 cm^{-1} was attributed to overlapping O–H stretching vibrations of the diol component and N–H stretching vibrations of IAA [40,42]. The peaks at 1371 and 1337 cm^{-1} were assigned to vibrations associated with the aromatic indole ring, whereas the band at 1601 cm^{-1} was attributed to N–H bending vibrations. Compared with pure IAA, the appearance of new absorption bands and shifts in characteristic frequencies confirmed the successful synthesis of the ICAE hydrogel.

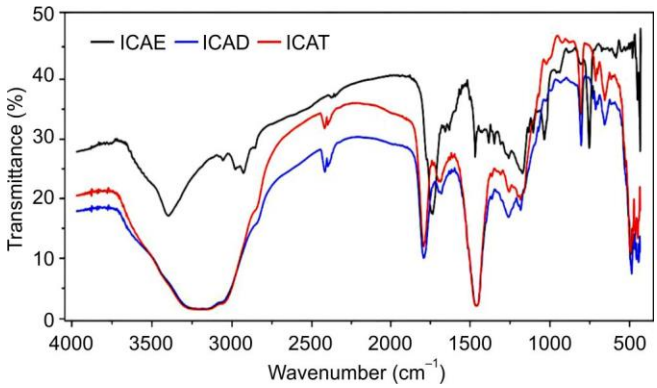

Fig. 1. FT-IR spectra of ICAE, ICAD and ICAT hydrogels

The FT-IR spectrum of ICAD displayed a prominent band at 1623 cm^{-1} indicating the presence of carboxylic acid groups derived from citric acid. The esterification reaction was evidenced by the appearance of a strong C=O stretching band at 1734 cm^{-1} and a C–O–C stretching band at 1020 cm^{-1}. The COO^- stretching vibration was observed at 1401 cm^{-1}. The characteristic -CH_2- stretching bands of the polyester backbone were also detected, with aliphatic C–H stretching vibrations appearing at 2362 and 2343 cm^{-1}. The incorporation of IAA was confirmed by the aromatic C=C stretching band at 1623 cm^{-1} and the characteristic indole C–H out-of-plane bending vibration at 744 cm^{-1}. A broad absorption band at 3159 cm^{-1} was attributed to overlapping O–H and N–H stret-

ching vibrations from the diol and IAA components, respectively. The band at 1601 cm^{-1} corresponded to N–H bending vibrations. These characteristic spectral features verified the successful formation of the ICAD hydrogel.

Similarly, the FT-IR spectrum of ICAT exhibited a band at 1623 cm^{-1} corresponding to the carboxylic acid group of citric acid. The ester linkage formation was confirmed by the appearance of a C=O stretching band at 1735 cm^{-1} and a C–O–C stretching band at 1124 cm^{-1}. The COO^- stretching vibration was observed at 1401 cm^{-1}, while the aliphatic C–H stretching vibration appeared at 2363 cm^{-1} [41]. The successful incorporation of IAA was evidenced by the aromatic C=C stretching band at 1623 cm^{-1} and the characteristic indole C–H out-of-plane bending vibration at 747 cm^{-1}. A broad absorption band centered at 3159 cm^{-1} was assigned to overlapping O–H and N–H stretching vibrations arising from the diol and IAA components. The peak at 1290 cm^{-1} was attributed to vibrations associated with the indole moiety, while the band at 1636 cm^{-1} corresponded to N–H bending vibrations. The observed spectral shifts and characteristic absorption bands confirmed the successful synthesis and structural integrity of the ICAT hydrogel.

NMR spectral studies: The ^{1}H NMR spectrum of the ICAE hydrogel (Fig. 2) exhibited a signal at δ 4.1 ppm, which was attributed to the hydroxyl (–OH) protons of the diol component [43]. Multiple resonances observed in the region of δ 7.0-7.5 ppm corresponded to the aromatic protons of the indole ring derived from indole-3-acetic acid (IAA) [44]. The characteristic signal at 10.9 ppm was assigned to the indole N–H proton, indicating that the indole moiety remained intact during hydrogel formation. Furthermore, the disappearance of the carboxylic acid proton signal originally observed at approximately δ 12.2 ppm provided strong evidence for esterification and successful hydrogel formation.

Similarly, the ^{1}H NMR spectrum of the ICAD hydrogel displayed multiple peaks in the range of δ 6.9-7.5 ppm corresponding to the aromatic protons of the indole ring. The signal at δ 10.9 ppm was attributed to the indole N–H proton, confirming the preservation of the indole structure after polymerisation. A resonance at δ 4.1 ppm was assigned to the hydroxyl protons of the diol component. The solvent signal appeared at δ 3.5-3.6 ppm, while the disappearance of the carboxylic acid proton signal at approximately δ 12.4 ppm, confirmed the successful esterification and formation of the ICAD hydrogel.

The ^{1}H NMR spectrum of the ICAT hydrogel also exhibited a characteristic signal at δ 4.1 ppm corresponding to the hydroxyl protons of the diol unit. Multiplet signals observed between δ 6.9 and 7.5 ppm were assigned to the aromatic protons of the indole ring from IAA. The N–H proton resonance appeared in the range of δ 10.7-10.9 ppm, suggesting that the indole functionality remained unchanged during hydrogel synthesis. The absence of the carboxylic acid proton signal at approximately δ 12.2 ppm further confirmed the successful esterification reaction and formation of the ICAT hydrogel.

SEM studies: The SEM micrograph of the ICAE hydrogel (Fig. 3) revealed an irregular and rough surface morphology with a comparatively smooth and less porous interior structure. Such a morphology facilitates fluid penetration into

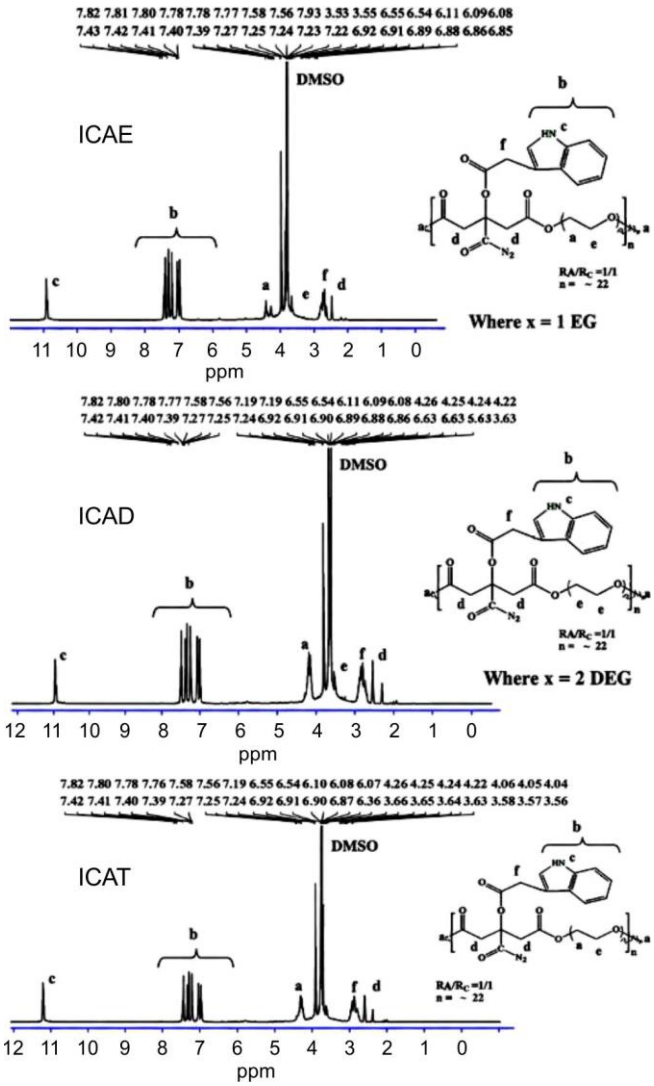

Fig. 2. ^{1}H NMR spectra ICAE, ICAD and ICAT hydrogels

the hydrogel matrix under different pH conditions, thereby enhancing its swelling capacity. In contrast, the more homogeneous surface morphology observed for the ICAD and ICAT hydrogels may account for their relatively lower swelling equilibrium. The moon- and leaf-like surface features observed in the SEM images are indicative of hydrophobic domains, which may contribute to the reduced swelling behaviour of the polymeric hydrogels [45].

Thermal studies: The thermal stability of the synthesised hydrogels was evaluated by TGA and the corresponding thermograms are shown in Fig. 4. The ICAE hydrogel exhibited a three-stage decomposition pattern. The first stage occurred at approximately 200 ºC with a weight loss of about 26%, followed by a second stage around 290 ºC with a 22% weight loss and a third stage near 350 ºC with an additional 18% weight loss. In contrast, the ICAD hydrogel showed two major decomposition stages: the first between 100 and 270 ºC with an average weight loss of 28% and the second between 280 and 380 ºC with an average weight loss of 41%. Similarly, the ICAT hydrogel exhibited an initial decomposition stage at ~200 ºC with a weight loss of 28%, followed by a second decomposition stage around 250 ºC with a weight loss of 34%.

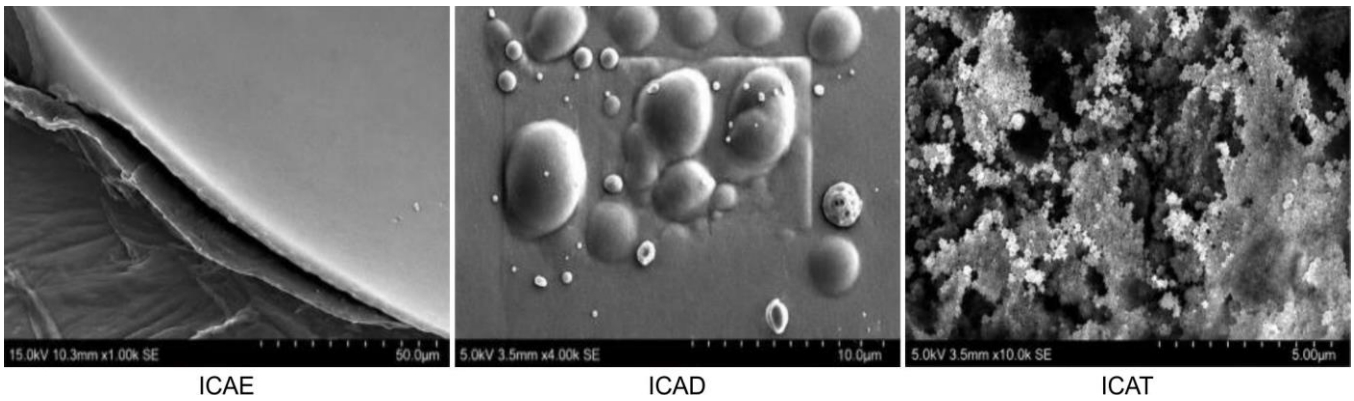

Fig. 3. SEM images of ICAE, ICAD and ICAT hydrogels

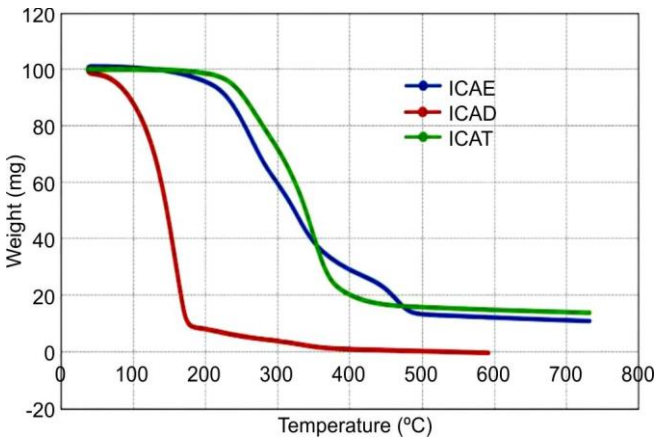

Fig. 4. Thermograms of ICAE, ICAD and ICAT hydrogels

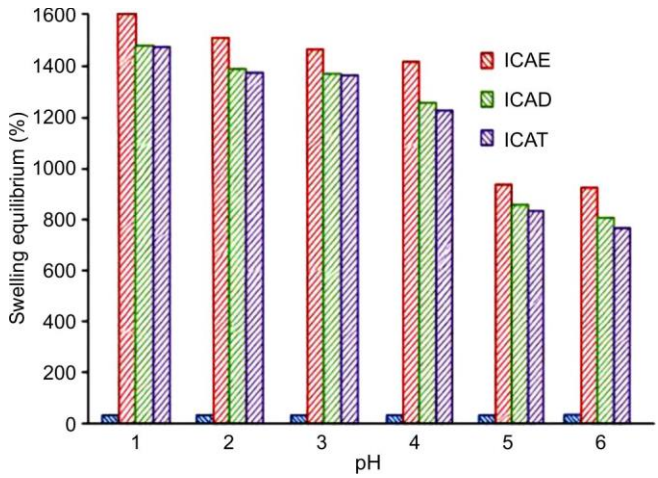

Fig. 5. Swelling equilibrium (%) of ICAE, ICAD and ICAT hydrogels in buffer solutions of different pHs after 48 h of immersion

For all hydrogels, the initial weight loss was attributed to the evaporation of physically adsorbed and bound water molecules within the hydrogel matrix. The subsequent decomposition stages were associated with the cleavage of polymer chains, degradation of ester linkages, breakdown of indole moieties and carbonization of the polymeric network. Among the synthesised hydrogels, ICAE exhibited the highest thermal stability, as evidenced by its higher decomposition temperatures and more gradual weight-loss profile. This enhanced thermal resistance may be attributed to the optimal structural balance and stronger intermolecular interactions within the ICAE network, which impart greater stability to the polymer backbone [46].

Swelling studies of hydrogels: The swelling equilibrium behaviour of the IAA-based hydrogels was evaluated in buffer solutions of varying pH (3.0, 4.0, 6.0, 7.0, 9.0 and 10.0) after 48 h of immersion, and the swelling equilibrium percentage (S_{eq}%) was calculated using eqn. 1. As shown in Fig. 5, all hydrogels exhibited higher swelling in acidic media than in alkaline conditions. This behaviour can be attributed to the ionization of the carboxylic acid groups of citric acid (pK_a = 3.14) and the protonation of functional groups associated with IAA (pK_a = 4.75). At acidic pH, increased osmotic pressure and electrostatic repulsion within the polymer network promoted greater water uptake, resulting in enhanced swelling of the hydrogels [47].

The ICAE (IAA-EG-CA) hydrogel exhibited Seq% values of 1600, 1500, 1453, 1400, 900 and 880% at pH 3.0, 4.0, 6.0, 7.0, 9.0 and 10.0, respectively. Similarly, the ICAD (IAA-DEG-CA) hydrogel showed S_{eq}% values of 1463, 1370, 1353, 1230, 820 and 790%, while the ICAT (IAA-TEG-CA) hydrogel displayed S_{eq}% values of 1450, 1355, 1342, 1200, 800 and 740% at the corresponding pH values.

The swelling behaviour was strongly influenced by the diol chain length in the hydrogel network. As the chain length increased from ethylene glycol (EG) to triethylene glycol (TEG), the swelling equilibrium decreased across all pH conditions. Among the synthesized hydrogels, ICAE exhibited the highest swelling capacity, followed by ICAD and ICAT. Thus, the swelling equilibrium decreased with increasing diol chain length and followed the order ICAE > ICAD > ICAT, suggesting that shorter diol chains facilitate enhanced water absorption and swelling of the hydrogel network.

Biological studies

Antifungal studies: The antifungal efficacy of all synthesised ICAE, ICAD and ICAT hydrogels increased with increasing concentration, indicating a dose-dependent response. Among the tested formulations, ICAE hydrogel exhibited the highest antifungal activity, producing zones of inhibition of 18, 15 and 14 mm against *A. fumigatus*, *C. albicans* and *R. oryzae*, respectively, at 2000 µg/mL. ICAD hydrogel also demonstrated appreciable activity, with inhibition zones of 16, 15 and 12 mm against the respective fungal strains, while

ICAT hydrogel showed comparatively lower but significant antifungal effects, yielding inhibition zones of 14, 13 and 11 mm, respectively, at the same concentration. Fig. 6 clearly indicate that all hydrogels possess broad-spectrum antifungal potential, with *A. fumigatus* being the most susceptible strain. The enhanced antifungal performance of ICAE and ICAD hydrogels can be attributed to the synergistic influence of electron-withdrawing groups such as aromatic rings and -COOH functionalities, together with electron-donating groups including $–CH_2$, –NH and –OH, which facilitate stronger interactions with fungal cell components. Furthermore, the superior activity observed for ICAE, followed by ICAD and ICAT hydrogels, may also be associated with the higher abundance of acidic functional groups derived from citric acid and indole-3-acetic acid, which contribute to improved antimicrobial efficacy through enhanced surface reactivity and disruption of fungal cellular processes [48].

Cytotoxic activity: Cytotoxicity assay of ICAE, ICAD, and ICAT hydrogels was evaluated using the MTT assay at concentrations of 25, 50, 100, 250 and 500 μg/mL. The ICAE hydrogel exhibited cell viability rates of 100%, 98%, 90%, 87% and 86%, respectively, across the tested concentration range. Similarly, ICAD hydrogels demonstrated cell viability values of 100%, 97%, 92%, 88% and 86% at corresponding concentrations, indicating their non-cytotoxic nature. ICAT hydrogels showed cell viability rates of 100%, 100%, 92%, 91% and 88% at concentrations of 25, 50, 100, 250 and 500 μg/mL, respectively, further confirming their excellent biocompatibility (Fig. 7).

Thus, all three hydrogel formulations (ICAE, ICAD and ICAT) maintained cell viability above 80% even at 500 μg/mL, confirming their non-cytotoxic nature and excellent biocompatibility. The high viability values also suggest their suitability for supporting cellular proliferation and migration in biomedical applications. Furthermore, cell viability remained well above 50% across the entire concentration range tested. As viability did not decrease to 50% even at 500 μg/mL, the IC_{50} value could not be determined experimentally and

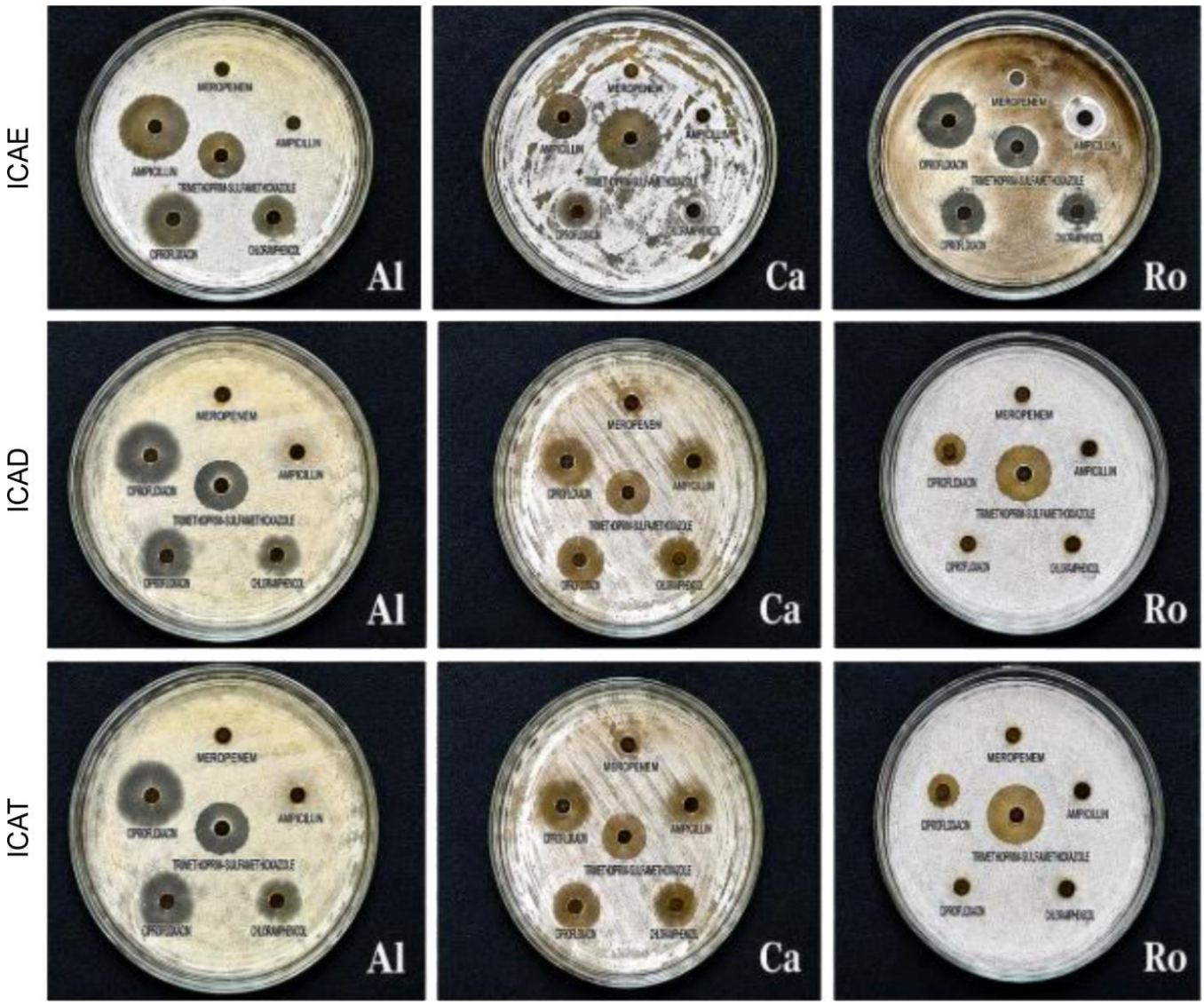

Fig. 6. Antifungal activity of ICAE, ICAD and ICAT hydrogels against *A. niger* (Al), *C. albicans* (Ca) and *R. oryzae* (Ro) at different concentrations

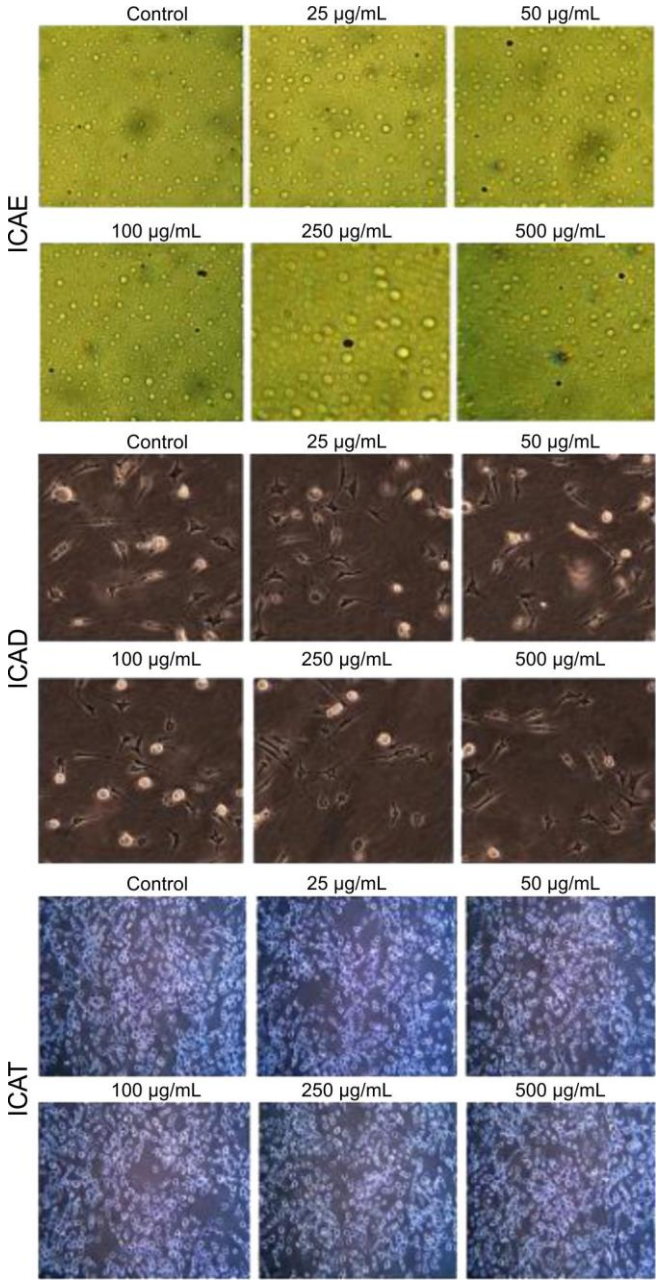

Fig. 7. MTT assay images of ICAE, ICAD and ICAT hydrogels at different concentrations

is estimated to be higher than 500 µg/mL for all formulations. These findings demonstrate the low cytotoxicity and favourable biocompatibility of the developed hydrogels [49].

Wound healing application: The wound-healing potential of all the three hydrogels was evaluated using the scratch assay by monitoring wound closure over time. Wound healing is closely associated with cell migration, proliferation, cytocompatibility, and the antimicrobial properties of hydrogels [50]. ICAE exhibited wound closure rates of 30%, 55%, and 75% after 24, 48 and 72 h, respectively. Similarly, ICAD showed wound closure of 34%, 55%, and 64%, while ICAT demonstrated 37%, 41% and 48% at the corresponding time intervals (Fig. 8).

The continuous reduction in scratch width indicates enhanced fibroblast migration and proliferation, which are essential for tissue regeneration and wound repair [51]. Free radicals can damage membrane lipids through oxidation, impairing cellular functions and delaying healing; therefore, antioxidant materials can facilitate wound recovery [45]. The non-cytotoxic nature of the hydrogels, confirmed by the MTT assay, supported cell migration and wound closure. Moreover, the high swelling capacity and water absorption ability of ICAE promote rapid uptake of wound exudates, creating a favourable healing environment [52,53]. The negative sign in Table-1 denotes the absence of wound-closure activity [54]. Among all formulations, ICAE exhibited the best wound-healing performance, attributed to its superior swelling behaviour and antioxidant, antibacterial and antifungal properties [55].

TABLE-1
WOUND CLOSURE VALUES OF HYDROGELS FOR 3 days

Sample	0 h	24 h	48 h	72 h
Control	-0.26	14.42	26.67	23.27
ICAE	-1.00	46.48	63.13	63.30
ICAD	-0.53	32.51	55.04	79.78
ICAT	0.32	45.09	37.52	33.79

Anticancer activity: The anticancer activity of ICAE, ICAD and ICAT hydrogels against A549 cells was evaluated using the MTT assay. ICAE hydrogel exhibited cancer cell viability of 80%, 79%, 77%, 72% and 69% at concentrations of 25, 50, 100, 250 and 500 µg/mL, respectively, with an IC_{50} value of 138 µg/mL. The relatively lower cell viability observed for ICAE indicates enhanced growth inhibition of A549 cells while maintaining acceptable biocompatibility at lower concentrations. Similarly, ICAD hydrogel showed cell viability values of 90%, 91%, 83%, 74% and 71% at corresponding concentrations, whereas ICAT exhibited viability of 100%, 95%, 91%, 87% and 84%. For both ICAD and ICAT, the IC_{50} values were estimated to be >500 µg/mL, indicating comparatively lower cytotoxic effects toward A549 cells.

Previous studies have reported a positive correlation between the antioxidant capacity of hydrogels and their anticancer activity, where enhanced free-radical scavenging ability contributes to the inhibition of cancer cell growth [56]. Among the tested formulations, ICAE demonstrated the strongest anticancer effect, as evidenced by its lower cell viability and IC_{50} value. The favourable biological performance of these hydrogels may be attributed to the strong interactions between citric acid and IAA within the hydrogel network, which contribute to their biocompatibility and potential antifungal and anticancer applications [5,57].

Conclusion

In this study, indole-3-acetic acid-based polyester hydrogels (ICAE, ICAD and ICAT) were successfully synthesized and characterized by FT-IR, ^{1}H NMR, SEM, TGA and swelling analyses. The hydrogels exhibited pH-responsive swelling behaviour, good thermal stability and significant antifungal activity. Cytotoxicity studies confirmed excellent biocompatibility, with cell viability exceeding 80% at all tested concentrations. Among the formulations, ICAE demonstrated the highest swelling capacity, superior wound-healing efficiency (75% closure at 72 h) and the strongest anticancer activity against

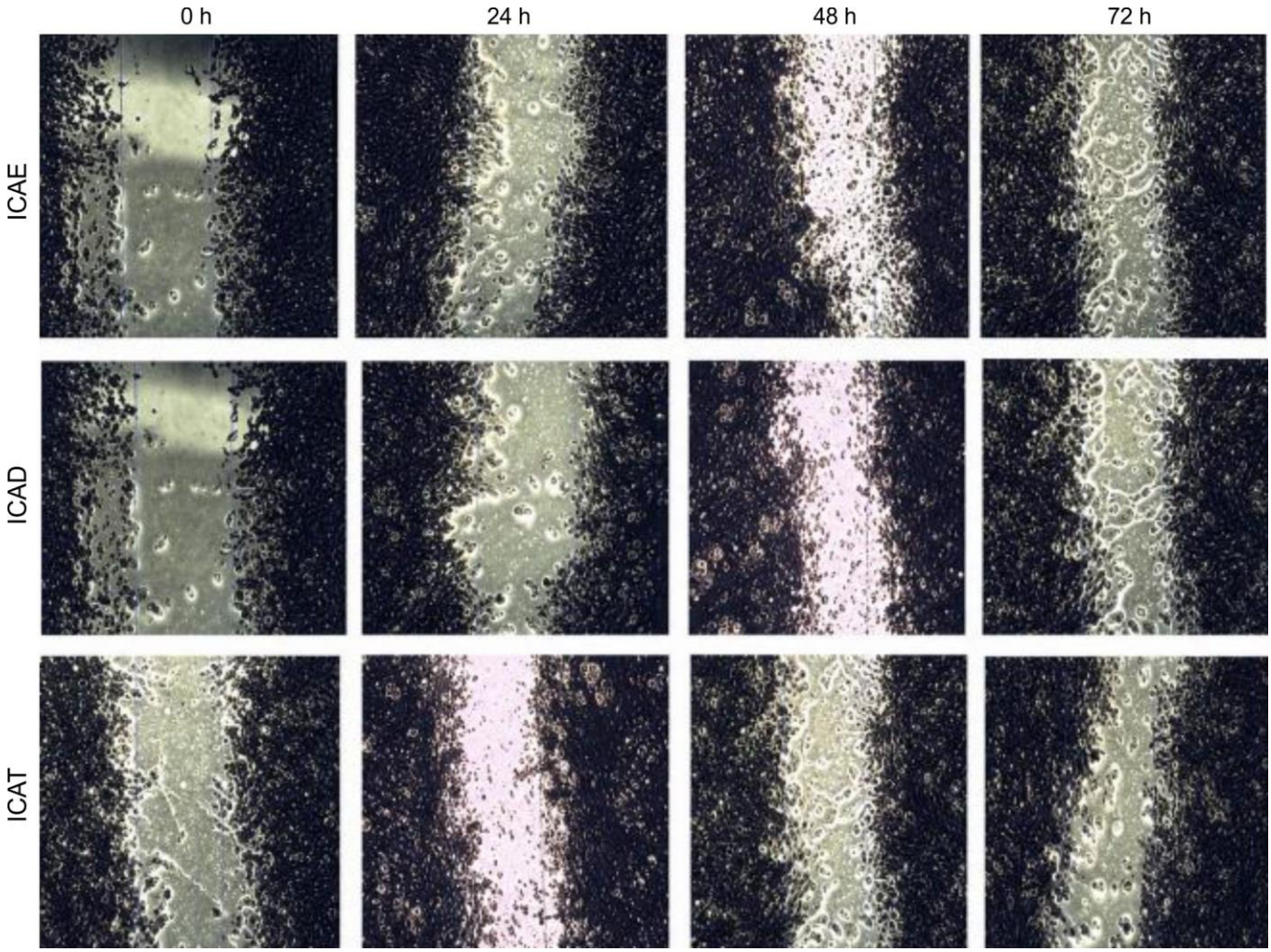

Fig. 8. Scratch assay images showing wound closure by ICAE, ICAD, and ICAT hydrogels at 0, 24, 48, and 72 h

A549 cells (IC_{50} = 138 μg/mL). These findings highlight the potential of ICAE as a multifunctional biomaterial for wound healing and biomedical applications.

CONFLICT OF INTEREST

The authors declare that there is no conflict of interests regarding the publication of this article.

DECLARATION OF AI-ASSISTED TECHNOLOGIES

During the preparation of this manuscript, the authors used an AI-assisted tool(s) to improve the language. The authors reviewed and edited the content and take full responsibility for the published work.

REFERENCES

1. E.M. Ahmed, F.S. Aggor, A.M. Awad and A.T. El-Aref, *Carbohydr. Polym.*, **91**, 693 (2013); https://doi.org/10.1016/j.carbpol.2012.08.056
2. W.A. Laftah, S. Hashim and A.N. Ibrahim, *Polym. Plast. Technol. Eng.*, **50**, 1475 (2011); https://doi.org/10.1080/03602559.2011.593082
3. P.I. Lee, *J. Controlled Rel.*, **17**, 297 (1991); https://doi.org/10.1016/0168-3659(91)90148-7
4. Y. Li, G. Huang, X. Zhang, B. Li, Y. Chen, T. Lu, T.J. Lu and F. Xu, *Adv. Funct. Mater.*, **23**, 660 (2013); https://doi.org/10.1002/adfm.201201708
5. G. Chitra, D.S. Franklin, S. Sudarsan, M. Sakthivel and S. Guhanathan, *Int. J. Biol. Macromol.*, **95**, 363 (2017); https://doi.org/10.1016/j.ijbiomac.2016.11.068
6. S. Burkert, T. Schmidt, U. Gohs, H. Dorschner and K.-F. Arndt, *Radiat. Phys. Chem.*, **76**, 1324 (2007); https://doi.org/10.1016/j.radphyschem.2007.02.024
7. W. Zhao, X. Jin, Y. Cong, Y. Liu and J. Fu, *J. Chem. Technol. Biotechnol.*, **88**, 327 (2013); https://doi.org/10.1002/jctb.3970
8. T. Iizawa, H. Taketa, M. Maruta, T. Ishido, T. Gotoh and S. Sakohara,, *J. Appl. Polym. Sci.*, **104**, 842 (2007); https://doi.org/10.1002/app.25605
9. L. Yang, J.S. Chu and J.S. Fix, *Int. J. Pharm.*, **235**, 1 (2002); https://doi.org/10.1016/S0378-5173(02)00004-2
10. Z. Maolin, L. Jun, Y. Min and H. Hongfei, *Radiat. Phys. Chem.*, **58**, 397 (2000); https://doi.org/10.1016/S0969-806X(99)00491-0
11. M.C. Hacker and A.G. Mikos, in eds.: A. Atala, R.P. Lanza, J.A. Thomson and R.M. Nerem, Synthetic Polymers, In: Principles of Regenerative Medicine, Eds. San Diego, CA, USA: Academic Press, edn. 2, pp. 587–622 (2011).
12. J. Shin, P.V. Braun and W. Lee, *Sens. Actuators B Chem.*, **150**, 183 (2010); https://doi.org/10.1016/j.snb.2010.07.018
13. O. Wichterle and D. Lim, *Nature*, **185**, 117 (1960); https://doi.org/10.1038/185117a0

14. R. Salihu, S.I. Abd Razak, N.A. Zawawi, M.R.A. Kadir, N.I. Ismail, N. Jusoh, M.R. Mohamad and N.H.M. Nayan, *Eur. Polym. J.*, **146**, 110271 (2021); https://doi.org/10.1016/j.eurpolymj.2021.110271
15. A.K. Saxena, *J. Thorac. Cardiovasc. Surg.*, **139**, 496 (2010); https://doi.org/10.1016/j.jtcvs.2008.11.003
16. S. Goel, S. Dubey, S. Sharma and J. Jacob, *Eur. Polym. J.*, **162**, 110919 (2022); https://doi.org/10.1016/j.eurpolymj.2021.110919
17. K. Wang, Q. Fu, X. Chen, Y. Gao and K. Dong, *RSC Adv.*, **2**, 7772 (2012); https://doi.org/10.1039/C2RA20989F
18. D.S. Franklin and S. Guhanathan, *Ecotoxicol. Environ. Saf.*, **121**, 80 (2015); https://doi.org/10.1016/j.ecoenv.2015.05.003
19. F. Yang, Z. Bao, Z. Li, S. Li, J. Ren, X. Wu and J. Huang, *Cell Rep. Phys. Sci.*, **7**, 103311 (2026); https://doi.org/10.1016/j.xcrp.2026.103311
20. S. Sudarsan, D.S. Franklin, M. Sakthivel and S. Guhanathan, *Carbohydr. Polym.*, **148**, 206 (2016); https://doi.org/10.1016/j.carbpol.2016.04.060
21. G. He, C. Zhu, S. Ye, W. Cai, Y. Yin, H. Zheng and Y. Yi, *Int. J. Biol. Macromol.*, **91**, 828 (2016); https://doi.org/10.1016/j.ijbiomac.2016.05.091
22. J.K. Patra, G. Das and K.-H. Baek, *J. Photochem. Photobiol. B*, **161**, 200 (2016); https://doi.org/10.1016/j.jphotobiol.2016.05.021
23. Y. Kuthati, R.K. Kankala, S.X. Lin, C.F. Weng and C.H. Lee, *Mol. Pharm.*, **12**, 2289 (2015); https://doi.org/10.1021/mp500836w
24. P.I. Siafaka, A.P. Zisi, M.K. Exindari, I.D. Karantas and D.N. Bikiaris, *Carbohydr. Polym.*, **143**, 90 (2016); https://doi.org/10.1016/j.carbpol.2016.02.009
25. A.C.O. Gonzalez, T.F. Costa, Z.A. Andrade and A.R.A.P. Medrado, *An. Bras. Dermatol.*, **91**, 614 (2016); https://doi.org/10.1590/abd1806-4841.20164741
26. P.H. Wang, B.S. Huang, H.C. Horng, C.C. Yeh and Y.J. Chen, *J. Chin. Med. Assoc.*, **81**, 94 (2018); https://doi.org/10.1016/j.jcma.2017.11.002
27. D. Kiritsi and A. Nyström, *Mech. Ageing Dev.*, **172**, 51 (2018); https://doi.org/10.1016/j.mad.2017.11.004
28. S. Schreml, R.M. Szeimies, L. Prantl, M. Landthaler and P. Babilas, *J. Am. Acad. Dermatol.*, **63**, 866 (2010); https://doi.org/10.1016/j.jaad.2009.10.048.
29. M. Li, Y. Liang, J. He, H. Zhang and B. Guo, *Chem. Mater.*, **32**, 9937 (2020); https://doi.org/10.1021/acs.chemmater.0c02823
30. J. He, Y. Liang, M. Shi and B. Guo, *Chem. Eng. J.*, **385**, 123464 (2020); https://doi.org/10.1016/j.cej.2019.123464
31. M.J. Hall, S. Lopes-Ventura, M.V. Neto, J. Charneca, P. Zoio, M.C. Seabra, A. Oliva and D.C. Barral, *Pigment Cell Melanoma Res.*, **35**, 425 (2022); https://doi.org/10.1111/pcmr.13039
32. Y. Yang, Y. Liang, J. Chen, X. Duan and B. Guo, *Bioact. Mater.*, **8**, 341 (2022); https://doi.org/10.1016/j.bioactmat.2021.06.014
33. J. He, M. Shi, Y. Liang and B. Guo, *Chem. Eng. J.*, **394**, 124888 (2020); https://doi.org/10.1016/j.cej.2020.124888
34. H. Sung, J. Ferlay, R.L. Siegel, M. Laversanne, I. Soerjomataram, A. Jemal and F. Bray, *CA Cancer J. Clin.*, **71**, 209 (2021); https://doi.org/10.3322/caac.21660
35. J. Kaur, M. Gulati, N.K. Jha, J. Disouza, V. Patravale, K. Dua and S.K. Singh, *Drug Discov. Today*, **27**, 1495 (2022); https://doi.org/10.1016/j.drudis.2022.02.005
36. S. Arpicco, F. Dosio, B. Stella and L. Cattel, *Curr. Top. Med. Chem.*, **11**, 2346 (2011); https://doi.org/10.2174/156802611797183221
37. I. Nasibullin, I. Smirnov, P. Ahmadi, K. Vong, A. Kurbangalieva and K. Tanaka, *Nat. Commun.*, **13**, 39 (2022); https://doi.org/10.1038/s41467-021-27804-5
38. Y. Singh, M. Palombo and P. Sinko, *Curr. Med. Chem.*, **15**, 1802 (2008); https://doi.org/10.2174/092986708785132997
39. D.S. Franklin and S. Guhanathan, *J. Appl. Polym. Sci.*, **132**, 41403 (2015); https://doi.org/10.1002/app.41403
40. A.G. Ibrahim, F.A. Hai, H.A. Wahab and H. Mahmoud, *Am. J. Appl. Chem.*, **6**, 221 (2016).
41. M. Sadeghi, N. Ghasemi, M. Kazemi and F. Soleimani, *Middle-East J. Scientific Res.*, **11**, 311 (2012).
42. F. Cao, Z. Guan and D. Li, *J. Wuhan Univ. Technol. Mater. Sci. Ed.*, **23**, 513 (2008); https://doi.org/10.1007/s11595-007-4513-8
43. A. Wahl, N. Azaroual, M. Imbenotte, D. Mathieu, G. Forzy, B. Cartigny, G. Vermeersch and M. Lhermitte, *Toxicology*, **128**, 73 (1998); https://doi.org/10.1016/S0300-483X(98)00055-9
44. N. Chandimali, S.G. Bak, E.H. Park, H.-J. Lim, Y.-S. Won, E.-K. Kim, S.-I. Park and S.J. Lee, *Cell Death Discov.*, **24**, 19 (2025); https://doi.org/10.1038/s41420-024-02278-8
45. A. Pourjavadi and R.M. Gholam, *Turk. J. Chem.*, **30**, 595 (2006).
46. K. Hu, D. Zhao, G. Wu and J. Ma, *Polymer Chem.*, **6**, 7138 (2015); https://doi.org/10.1039/C5PY01075F
47. M. Kelen and N. Sanli, *J. Braz. Chem. Soc.*, **20**, 133 (2009); https://doi.org/10.1590/S0103-50532009000100021
48. D.R. Shah, R.P. Modh and K.H. Chikhalia, *Future Med. Chem.*, **6**, 463 (2014); https://doi.org/10.4155/fmc.13.212
49. M. Sánchez-Díez, P. Romero-Jiménez, N. Alegría-Aravena, C.E. Gavira-O'Neill, E. Vicente-García, J. Quiroz-Troncoso, R. González-Martos, C. Ramírez-Castillejo and J.M. Pastor, *Pharmaceutics*, **17**, 247 (2025); https://doi.org/10.3390/pharmaceutics17020247
50. K. Akhbari, A. Morsali and P. Retailleau, *Polyhedron*, **29**, 3304 (2010); https://doi.org/10.1016/j.poly.2010.09.011
51. S. Saeedi Garakani, S.M. Davachi, Z. Bagher, A. Heraji Esfahani, N. Jenabi, Z. Atoufi, M. Khanmohammadi, A. Abbaspourrad, H. Rashedi and M. Jalessi, *Int. J. Biol. Macromol.*, **164**, 356 (2020); https://doi.org/10.1016/j.ijbiomac.2020.07.138
52. M. Zhou, F. Lin, W. Li, L. Shi, Y. Li and G. Shan, *Int. J. Biol. Macromol.*, **166**, 1335 (2021); https://doi.org/10.1016/j.ijbiomac.2020.11.014
53. Y. Dong, M. Cui, J. Qu, X. Wang, S.H. Kwon, J. Barrera, N. Elvassore and G.C. Gurtner, *Acta Biomater.*, **108**, 56 (2020); https://doi.org/10.1016/j.actbio.2020.03.040
54. C.O. Okoli, A.C. Ezike, P.A. Akah, S.O. Udegbunam, T.C. Okoye, T.P. Mbanu and E. Ugwu, *Am. J. Pharmacol. Toxicol.*, **4**, 118 (2009); https://doi.org/10.3844/ajptsp.2009.118.126
55. K. Vimala, Y.M. Mohan, K.S. Sivudu, K. Varaprasad, S. Ravindra, N.N. Reddy, Y. Padma, B. Sreedhar and K. MohanaRaju, *Colloids Surf. B Biointerfaces*, **76**, 248 (2010); https://doi.org/10.1016/j.colsurfb.2009.10.044
56. B. Teong, C.-Y. Lin, S.-J. Chang, G. C.-C. Niu, C.-H. Yao, I.-F. Chen, and S.-M. Kuo, *J. Mater. Sci. Mater. Med.*, **26**, 49 (2015); https://doi.org/10.1007/s10856-014-5357-3
57. G. Chitra, D.S. Franklin, S. Sudarsan, M. Sakthivel and S. Guhanathan, *Polym. Bull.*, **74**, 3379 (2017); https://doi.org/10.1007/s00289-016-1900-3